



AFRL-RX-WP-JA-2016-0297

**MODELING THE ROLE OF BULK AND SURFACE
CHARACTERISTICS OF CARBON FIBER ON
THERMAL CONDUCTANCE ACROSS THE CARBON-
FIBER/MATRIX INTERFACE (POSTPRINT)**

Vikas Varshney, Ajit K. Roy, and Jeffery W. Baur

AFRL/RX

Vikas Varshney

UTC

21 September 2015

Interim Report

**Distribution Statement A.
Approved for public release: distribution unlimited.**

© 2015 AMERICAN CHEMICAL SOCIETY

(STINFO COPY)

**AIR FORCE RESEARCH LABORATORY
MATERIALS AND MANUFACTURING DIRECTORATE
WRIGHT-PATTERSON AIR FORCE BASE, OH 45433-7750
AIR FORCE MATERIEL COMMAND
UNITED STATES AIR FORCE**

REPORT DOCUMENTATION PAGE				Form Approved OMB No. 0704-0188	
<p>The public reporting burden for this collection of information is estimated to average 1 hour per response, including the time for reviewing instructions, searching existing data sources, gathering and maintaining the data needed, and completing and reviewing the collection of information. Send comments regarding this burden estimate or any other aspect of this collection of information, including suggestions for reducing this burden, to Department of Defense, Washington Headquarters Services, Directorate for Information Operations and Reports (0704-0188), 1215 Jefferson Davis Highway, Suite 1204, Arlington, VA 22202-4302. Respondents should be aware that notwithstanding any other provision of law, no person shall be subject to any penalty for failing to comply with a collection of information if it does not display a currently valid OMB control number. PLEASE DO NOT RETURN YOUR FORM TO THE ABOVE ADDRESS.</p>					
1. REPORT DATE (DD-MM-YY) 21 September 2015		2. REPORT TYPE Interim		3. DATES COVERED (From - To) 26 April 2012 – 21 August 2015	
4. TITLE AND SUBTITLE MODELING THE ROLE OF BULK AND SURFACE CHARACTERISTICS OF CARBON FIBER ON THERMAL CONDUCTANCE ACROSS THE CARBON-FIBER/MATRIX INTERFACE (POSTPRINT)				5a. CONTRACT NUMBER FA8650-11-D-5800-0003	
				5b. GRANT NUMBER	
				5c. PROGRAM ELEMENT NUMBER 61102F	
6. AUTHOR(S) 1) Vikas Varshney, Ajit K. Roy, and Jeffery W. Baur - AFRL/RX 2) Vikas Varshney - UTC				5d. PROJECT NUMBER 3002	
				5e. TASK NUMBER 0003	
				5f. WORK UNIT NUMBER X0HA	
7. PERFORMING ORGANIZATION NAME(S) AND ADDRESS(ES) 1) AFRL/RX Wright-Patterson AFB, OH 45433 2) Universal Technology Corporation, 1270 N. Fairfield Rd, Dayton, OH 45432-2636				8. PERFORMING ORGANIZATION REPORT NUMBER	
9. SPONSORING/MONITORING AGENCY NAME(S) AND ADDRESS(ES) Air Force Research Laboratory Materials and Manufacturing Directorate Wright-Patterson Air Force Base, OH 45433-7750 Air Force Materiel Command United States Air Force				10. SPONSORING/MONITORING AGENCY ACRONYM(S) AFRL/RXCCM	
				11. SPONSORING/MONITORING AGENCY REPORT NUMBER(S) AFRL-RX-WP-JA-2016-0297	
12. DISTRIBUTION/AVAILABILITY STATEMENT Distribution Statement A. Approved for public release: distribution unlimited.					
13. SUPPLEMENTARY NOTES PA Case Number: 88ABW-2015-4454; Clearance Date: 21 Sep 2015. This document contains color. Journal article published in ACS Applied Materials Interfaces, Vol. 7, No. 48, 9 November 2015. © 2015 American Chemical Society. The U.S. Government is joint author of the work and has the right to use, modify, reproduce, release, perform, display, or disclose the work. The final publication is available at DOI: 10.1021/acsami.5b08591					
14. ABSTRACT (Maximum 200 words) The rapid heating of carbon-fiber-reinforced polymer matrix composites leads to complex thermophysical interactions which not only are dependent on the thermal properties of the constituents and microstructure but are also dependent on the thermal transport between the fiber and resin interfaces. Using atomistic molecular dynamics simulations, the thermal conductance across the interface between a carbon-fiber near-surface region and bismaleimide monomer matrix is calculated as a function of the interface and bulk features of the carbon fiber. The surface of the carbon fiber is modeled as sheets of graphitic carbon with (a) varying degrees of surface functionality, (b) varying defect concentrations in the surface-carbon model (pure graphitic vs partially graphitic), (c) varying orientation of graphitic carbon at the interface, (d) varying interface saturation (dangling vs saturated bonds), (e) varying degrees of surface roughness, and (f) incorporating high conductive fillers (carbon nanotubes) at the interface. After combining separately equilibrated matrix system and different surface-carbon models, thermal energy exchange is investigated in terms of interface thermal conductance across the carbon fiber and the matrix.					
15. SUBJECT TERMS BMI resin; carbon fibers; interfaces; molecular dynamics; thermal conductance					
16. SECURITY CLASSIFICATION OF:			17. LIMITATION OF ABSTRACT: SAR	18. NUMBER OF PAGES 12	19a. NAME OF RESPONSIBLE PERSON (Monitor) Jeffery Baur 19b. TELEPHONE NUMBER (Include Area Code) (937) 255-3622
a. REPORT Unclassified	b. ABSTRACT Unclassified	c. THIS PAGE Unclassified			

Modeling the Role of Bulk and Surface Characteristics of Carbon Fiber on Thermal Conductance across the Carbon-Fiber/Matrix Interface

Vikas Varshney,^{*,†,‡} Ajit K. Roy,[†] and Jeffery W. Baur^{*,†}

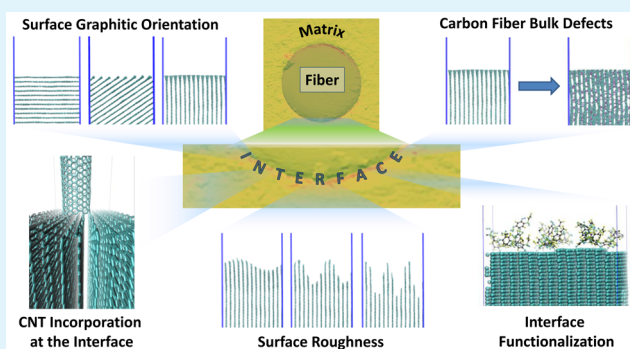
[†]Materials and Manufacturing Directorate, Air Force Research Laboratory, Wright-Patterson Air Force Base, Ohio 45433-7749, United States

[‡]Universal Technology Corporation, Dayton, Ohio 45432-2636, United States

S Supporting Information

ABSTRACT: The rapid heating of carbon-fiber-reinforced polymer matrix composites leads to complex thermophysical interactions which not only are dependent on the thermal properties of the constituents and microstructure but are also dependent on the thermal transport between the fiber and resin interfaces. Using atomistic molecular dynamics simulations, the thermal conductance across the interface between a carbon-fiber near-surface region and bismaleimide monomer matrix is calculated as a function of the interface and bulk features of the carbon fiber. The surface of the carbon fiber is modeled as sheets of graphitic carbon with (a) varying degrees of surface functionality, (b) varying defect concentrations in the surface-carbon model (pure graphitic vs partially graphitic), (c) varying orientation of graphitic carbon at the interface, (d) varying interface saturation (dangling vs saturated bonds), (e) varying degrees of surface roughness, and (f) incorporating high conductive fillers (carbon nanotubes) at the interface. After combining separately equilibrated matrix system and different surface-carbon models, thermal energy exchange is investigated in terms of interface thermal conductance across the carbon fiber and the matrix. It is observed that modifications in the studied parameters (a–f) often lead to significant modulation of thermal conductance across the interface and, thus, showcases the role of interface tailoring and surface-carbon morphology toward thermal energy exchange. More importantly, the results provide key bounds and a realistic degree of variation to the interface thermal conductance values at fiber/matrix interfaces as a function of different surface-carbon features.

KEYWORDS: carbon fibers, BMI resin, molecular dynamics, interfaces, thermal conductance



1. INTRODUCTION

Today, laser technology is being used in a wide variety of fields including communications, industrial and environmental applications, medicine, and materials' research and development (R&D). Some of the key areas in materials' R&D include mass spectral analysis using matrix-assisted laser desorption/ionization (MALDI)¹ and fabrication and machining of micro-/nano-patterned surfaces and thin films using pulsed or continuous lasers (such as fabrication of nanoelectronic devices and patterning of polymeric nanocomposites).^{2,3} Our specific interest lies in how different lasers interact with the polymeric composite materials, what parameters govern the interaction behavior, and how these laser–composite interactions lead to evolution of composites' thermophysical properties over time.

The basic mechanism of laser interaction with materials involves many nonequilibrium processes (thermal, mechanical, chemical, and physical) at varying length and time scales caused by fast deposition of laser energy and its dissipation in various forms.^{4,5} Because of the rapid heating rate, these non-

equilibrium processes cause spatial variability in thermophysical and mechanical properties of the matrix such as local heating, local matrix degradation due to sudden local increase in temperature, pressure wave formation, etc.^{4,5} In the context of polymeric composites, it is often desired to delay the onset of ablation and keep the composite intact by tailoring the interfaces between matrix and fillers (such as carbon fibers, carbon nanotubes, exfoliated graphite/graphene, and metallic nano-/micro-particles, etc.) by modulating the interactions between the two components. Since the ablation onset is primarily driven by a rise in temperature, it becomes crucial to understand individual thermal conduction characteristics of the matrix and fillers (thermal conductivity), as well as of their mutual interface (interface thermal conductance).

Received: September 11, 2015

Accepted: November 9, 2015

Published: November 9, 2015

Within the framework of carbon-fiber-based nano-/micro-composites, several experimental techniques (laser flash, photoacoustic, 3ω , thermoreflectance, infrared microscopy, etc.) have been employed to measure the thermal conductivity of individual components as well as the “effective” thermal conductivity of the nanocomposites.^{6,7} However, because of the small length scales involved, it has been significantly challenging to directly and accurately measure the nanocomposite interface features, both morphological (roughness, interfacial bonding nature, fractional contact area, etc.) and thermal transport characteristics. Most of the experimentally reported values of interface thermal conductance for carbon-based nanocomposites are evaluated indirectly (fitting the measured experimental data using different mathematical models, often requiring thermal properties of individual components as input parameters).^{8–14}

On the contrary, because of the sharpness of molecular interfaces, atomistic molecular dynamics (MD) simulations¹⁵ offer an alternative as well as a direct approach to calculate the thermal energy exchange across matrix/filler interfaces in terms of interface thermal conductance. In these simulations, only the details of microscopic interactions need to be specified (often extracted using quantum chemical calculations) and no further assumptions need to be made in order to investigate the equilibrium or nonequilibrium phenomenon happening at these time scales. To date, within the framework of carbon/polymeric interfaces, most molecular modeling reports have estimated thermal conductance primarily with either carbon nanotubes or single/few-layer graphene (1–2 nm fillers).^{14,16–30} Furthermore, in many of these studies, interface functionalization has been used as the key parameter to tailor the interfacial thermal transport characteristics.^{18,20,23,24,27,29,30}

In principle, apart from interface functionalization, several other parameters could be altered to modulate the thermal transport across carbon-fiber/matrix interfaces. This could include *interface characteristics* such as interface roughness, the nature of dangling bonds, incorporation of high conductive fillers (nanotubes, metal nanoparticles) at the interface; *carbon-fiber characteristics* such as its amorphous or graphitic nature and graphitic orientation near the interface; and *matrix features* such as degree of curing, local crystallinity, or molecular order near the interface, etc. To the best of the authors’ knowledge, these parameters have either not been explored or been explored in a very limited way from the perspective of interface thermal conductance across carbon-fiber/matrix interfaces.

This work addresses several of the highlighted issues to (a) model different types of carbon-fiber surface models ranging between ~ 5 and ~ 17 nm (mimicking the near-surface region of carbon fiber to a much larger scale than what is reported to date); (b) model high-temperature BMI monomeric resins (specifically Matrimid BMI-5292 because of its high temperature stability) with atomistic resolution; and (c) model the effect of the aforementioned parameters (including functionalization) on carbon-fiber/BMI-matrix interfacial thermal transport in a single comprehensive study.

It is important to point out that while modeling thermal transport across carbon-fiber/crosslinked resin is ideal, the following study investigates the transport characteristics across its uncrosslinked counterpart because of the following reasons. (A) Cross-linking reactions in BMI are notably more complex than well-studied epoxy-based resins. For example, unlike curing in epoxy, BMI curing consists of five different reaction pathways;^{31,32} (B) Specific reaction pathways are temperature

dependent, and their relative importance to experimental conditions are not well-quantified. (C) Inclusion of cross-linking would significantly broaden the scope of the investigation, i.e., investigating the effect of the degree of curing and the effect of different reactions and their relative occurrence on investigated properties, etc. We do, however, discuss the possible modulation of interfacial thermal transport because of curing phenomenon toward the end of the article. Understanding thermal transport across the carbon-fiber and monomeric matrix interface is also pertinent from the perspective of laser-assisted curing of carbon-fiber composites. Here, the interfacial thermal transport is expected to govern the heat flow from carbon fiber to the matrix (most of the laser energy is absorbed by the carbon fiber), subsequently determining the temperature rise and distribution in the monomeric matrix and thus affecting its curing kinetics.^{31,32}

2. SIMULATION SETUP AND METHODOLOGY

The section is divided into five subsections, dealing with the (a) preparation of BMI matrix, (b) preparation of different surface-carbon and (c) interface models, (d) preparation of combined systems for thermal conductance calculations, and (e) simulation methodology for thermal conductance calculations.

2.1. Matrix Preparation. The BMI resin (Matrimid BMI-5292) is composed of 4,4'-bismaleimidodiphenyl methane (BMPM) and *O,O'*-diallylbisphenol A (DABPA) monomers, often in a 1:1 molar ratio.^{33,34} The schematic representations of these monomers, along with their molecular structures, are shown in Figure 1. As a part of the initial

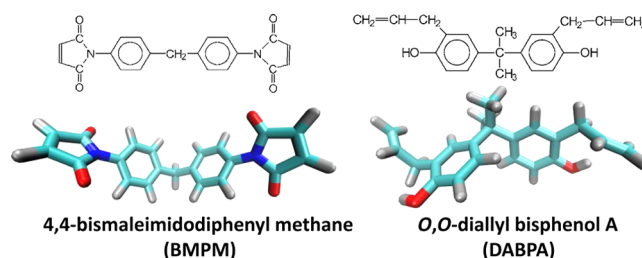


Figure 1. Molecular structure and schematic representation of the two monomer components of the Matrimid BMI-5292 resin. Color scheme: cyan, carbon; blue, nitrogen; red, oxygen; silver, hydrogen.

simulation setup, these monomers were constructed in Materials Studio.³⁵ Among several all atom force fields tested (CVFF,³⁶ PCFF,³⁷ and GAFF^{38,39}) for successful generation of bonded and nonbonded parameters, only the general amber force field (GAFF) was able to generate all of the required parameters. Hence, GAFF parameters were employed to model the BMI matrix as well as all carbon-surface models for this study. It is often reported that when employing GAFF force field, restrained electrostatic potential (RESP) charges are best suited to model organic or biomolecules.^{38,39} For our simulations, RESP charge estimations and fittings were performed using GAUSSIAN09 software⁴⁰ and RESP code within the framework of the R.E.D. program.⁴¹ The LAMMPS package was employed to carry out all molecular dynamics simulations.⁴² For van der Waals interactions, a distance cutoff value of 12 Å was used while PPPM (particle–particle–particle mesh) technique was used to model long-range Columbic interactions as implemented in LAMMPS.

First, a system of ~ 9500 atoms was created by replicating both BMI monomers 108 times (total) along x -, y -, and z -directions. Following the initial minimization, MD simulations were carried out in NVT (canonical) ensemble to equilibrate the temperature at 300 K for 200 ps, followed by NPT (isothermal–isobaric) ensemble to equilibrate the density (and pressure) for 5 ns with independent barostats along the x -, y -, and z -directions. Afterward, 200 ps equilibration was performed in NVE (microcanonical) ensemble to confirm the energy

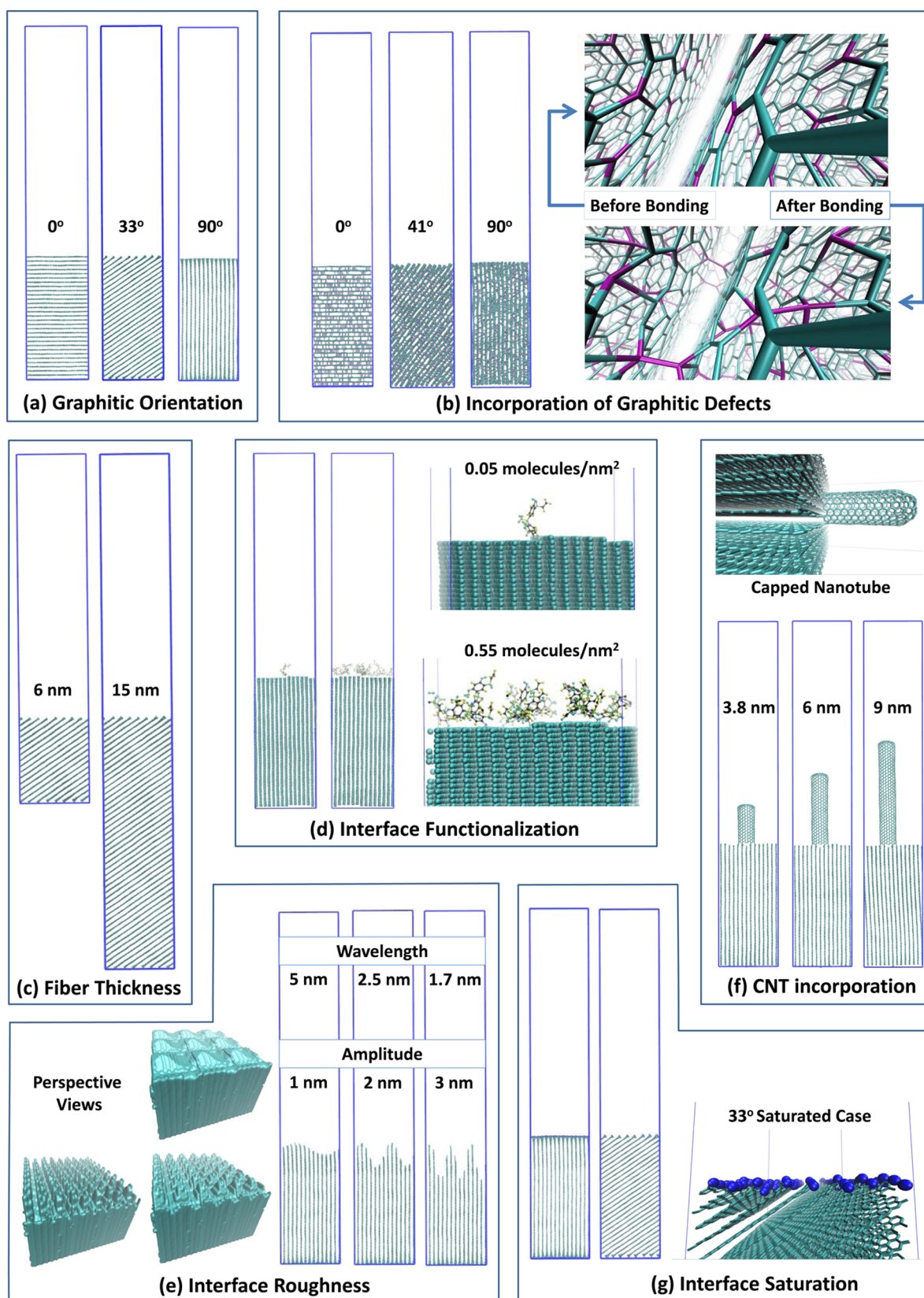


Figure 2. Several schematics of generated carbon-fiber surface models pertaining to (a) graphitic orientation; (b) incorporation of sp^3 defects within the graphitic structure (structure before and after bonding is also shown; purple, sp^3 carbon atoms; cyan, sp^2 carbon atoms); (c) effective fiber thickness; (d) interface functionalization (close-up interface region of two functionalized cases is also shown); (e) interface roughness with different roughness wavelengths and amplitude (perspective view is shown to reveal two-dimensional roughness features); (f) incorporation of bonded CNTs at the interface (close-up picture of nanotube cap is also shown); and (g) saturation of interface bonds (saturated H atoms are shown as blue spheres in close-up perspective).

conservation of the equilibrated system. For these simulations, periodic boundary conditions were employed in all three orthogonal directions to mimic bulk-like behavior. A time step of 1.0 fs was used during the equilibration phase. After successful equilibration, the system was subjected to a series of additional simulations for estimation and experimental comparison of the glass transition temperature, room temperature density, coefficient of thermal expansion, and thermal conductivity for the validation of the employed force field, which are reported elsewhere.⁴³

2.2. Carbon-Surface Models: Bulk Features Preparation.

Intrinsic carbon-fiber parameters such as graphitic order and its orientation with respect to heat flow direction, content of amorphous carbon within the carbon fiber, and sp^2/sp^3 bond ratio are important parameters which impact its bulk thermal transport characteristics. In principle, these parameters could also affect how interfaces of such fibers with organic matrices respond to an applied thermal gradient. In order to explore this, we generated several of such models incorporating differences in the aforementioned bulk carbon-fiber features which are discussed as follows.

2.2.1. Graphitic Orientation. In order to investigate the impact of graphitic layer orientation on interfacial thermal transport, several carbon-surface models were created with several different orientation angles of graphitic layers, ranging from 0° to 90° with respect to the x -direction (parallel to the interface). We will refer to these cases as C_θ , where θ represents the orientation angle of the graphitic layers with respect to the interface. Several models, with orientation angles of 0° , 8° , 16° , 24.5° , 33° , 41° , 51° , 66° , and 90° were created using in-house scripts with a fiber surface thickness of 10 nm. The details of building the carbon-surface models with different orientations are outlined in Supporting Information section S1. Figure 2a shows a few representative cases of carbon-surface models with graphitic orientations of C_0 , C_{33} , and C_{90} .

2.2.2. Incorporation of Defects. From the perspective of defects inclusion, pristine graphitic and amorphous carbon fibers represent two extremes of structural order. While models of pristine graphitic carbon are discussed in earlier text, interface thermal conductance across amorphous carbon and BMI matrix was recently modeled by us and is discussed elsewhere.⁴³ In this study, we create partially defective graphitic carbon-fiber surface models and investigate the effect of structural graphitic defects within carbon fibers on thermal conductance across fiber/matrix interfaces.

The defective graphitic carbon models can either be generated by incorporating defects in the pristine graphite or incorporating graphitic order starting from fully amorphous carbon.⁴⁴ For this study, the former route is chosen to create graphitic models with defects.⁴⁵ In this approach, we create interlayer bonding between carbon atoms and modify their hybridization from sp^2 to sp^3 . Here, we make use of the fact that, in AB layer stacking of graphite, there is one set of atom pair which lie on top of each other (looking along the c -axis), where atoms are 3.4 Å apart.⁴⁶ We randomly choose a predetermined number of such pairs (based on the final defect concentration), move atoms in each pair closer toward each other (1 Å each), and create a bond between the two. The bond creation is followed by updating the surrounding topology information (adding several new bond angles and dihedral angles and deleting two improper angles). By doing so, several models were created with volumetric defect concentrations ranging up to ~ 6 defects/nm³ for three graphitic orientations, namely, C_0 , C_{41} , and C_{90} , and are shown in Figure 2b, which also shows the structural changes before and after the bond creation for a representative case.

2.2.3. Fiber Surface Morphology Thickness. In order to explore the effect of thickness of fiber surface morphology (effective system size in MD simulations), several models were created with varying carbon-fiber thicknesses along the z -direction. Here, the C_{41} graphitic orientation model with thickness values ranging from 6 to 18 nm were created by deleting atoms on the boundaries of a much longer C_{41} model along the z -direction. Two of the created systems are shown in Figure 2c.

2.3. Carbon-Surface Models: Interface Features Preparation.

In addition to bulk carbon-fiber surface characteristics, interface

modification can also provide substantial modulation of interfacial thermal transport characteristics as evident from previous studies, mainly focused on functionalization.^{18,20,23,24,27,29,30} Below, we detail other interface modifications (in addition to functionalization) that can be employed to modify interface thermal conductance across fiber/matrix interfaces.

2.3.1. Functionalization. In order to investigate the effect of interface functionalization, five different carbon-surface models were created using graphitic orientation model C_{90} with a surface functionalization density ranging from 0.05 to 0.55 molecules/nm². Among different graphitic orientation models, the C_{90} model was chosen for interface functionalization studies because of two primary reasons; (a) in literature, most investigations dealing with the effect of interface functionalization on thermal conductance have been performed on C_0 type interfaces, such as the side wall of CNTs or surface modification in single-layer/few-layer graphene, and their outcomes are well-investigated; and (b) the C_{90} model provides the most number of possible functionalization sites because of the most number of edge carbon atoms among nonzero graphitic orientation models. For the C_{90} model, interface functionalization was carried out by bonding one of the monomers (DABPA) to the edge carbon atoms of a C_{90} carbon surface. In order to carry out bonding at the interface, first, a combined system of a BMI-matrix and C_{90} graphitic model was created. Then, a predetermined number of DABPA molecules were slowly dragged to the carbon-fiber surface over the course of an NVT MD simulation. Thereafter, bonds were created between the “hydroxyl O” (of DABPA) and “nearest edge carbon atom” using an in-house script, also updating new topology information (angles, dihedrals, and new force-field parameter assignment, etc.). The full procedure for functionalization and updating topology is outlined in detail in Supporting Information section S2. A few representative functionalized DABPA monomers (surrounding matrix removed for clarification) are shown in Figure 2d.

2.3.2. Roughness. The effect of carbon-fiber surface roughness on interfacial thermal transport was modeled by creating rough graphitic edges for a C_{90} graphitic system (Please see Supporting Information section S3 for specific details regarding generation of various roughness models). Here, nine carbon-surface models were created with varying sinusoidal roughness features (amplitude and wavelength) along both x - and y -directions. Specifically, roughness with three different amplitudes, i.e., 1, 2 and 3 nm, and 3 different wavelengths, i.e., ~ 1.7 , ~ 2.5 , and ~ 5 nm, were modeled. A few schematic carbon-surface models with varying roughness features are shown in Figure 2e.

2.3.3. CNT Incorporation at the Interface. In addition to functionalization and roughness, incorporating highly conductive nanofillers at the interface can also significantly modulate interfacial thermal transport. For example, CNTs grown directly in carbon fibers (also known as fuzzy carbon fibers) could provide additional surface area to interact with the matrix, potentially enhancing overall thermal transport characteristics. In order to mimic such an interface, several models were created by covalently bonding (10,10) end-capped single-wall CNTs of different lengths (~ 3.8 , ~ 6 , and ~ 9 nm) to a C_{90} carbon-surface model. The end-capping of the CNTs was achieved using NanoCap software.⁴⁷ The details of the bonding, such as how the junction was created along with other specific details, are outlined in Supporting Information section S4. The schematic representations of all three CNT bonded carbon-surface models are shown in Figure 2f.

2.3.4. Interface Saturation. From previous discussion, it should be noted that our graphitic carbon surface models (C_8 – C_{90}) have unsaturated or undersaturated valence for the edge atoms. In order to estimate if saturation of such valence could have significant impact on interfacial thermal transport, we saturated four of the nine graphitic models, namely, C_{16} , C_{33} , C_{51} , and C_{90} with hydrogen atoms for interface thermal conductance calculations. The visual differences between unsaturated and saturated surface-carbon atoms are shown in Figure 2g for the C_{33} graphitic model.

Afterward, each of the prepared carbon-surface models was subjected to equilibration in NVT, NPT, and NVE ensembles for

200, 2000, and 200 ps with time steps of 1, 1, and 0.5 fs, respectively, prior to combining with the matrix.

2.4. Combined Preparation. To calculate interface thermal conductance across the fiber/matrix interface, combined systems were created using relaxed BMI-matrix and separately equilibrated surface-carbon models (graphitic orientation, defects, fiber thickness, roughness, and interface saturation) to mimic the fiber/matrix interface (Figure 3a). We should point out that functionalized and CNT-

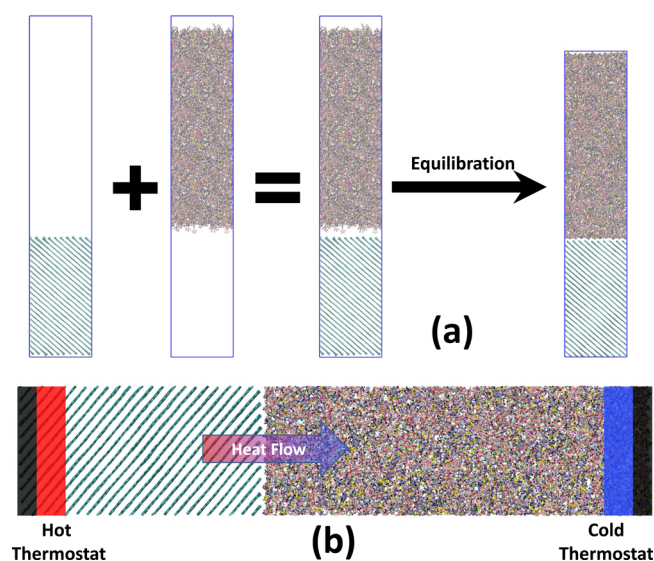


Figure 3. (a) Schematic representation of how the combined systems were prepared. It should be noted that the equilibrated structure (extreme left) has a lesser volume. (b) Schematic of nonequilibrium molecular dynamics simulations as employed in this investigation for a representative case. Color scheme: black, fixed atoms; red, hot thermostated atoms; blue, cold thermostated atoms. Thermal energy is directed from the graphitic carbon surface toward the matrix.

incorporated systems were combined during carbon-surface model preparations as discussed in Supporting Information sections S2 and S4, respectively. For the remaining cases, an in-house script was written to merge the two structures in order to generate the initial combined geometries. Within this code, the BMI matrix in the equilibrated slab-like geometry (4 times replication along the *z*-direction of the original system followed by its equilibration) was combined with the equilibrated carbon-surface models to generate initial coordinates for modeling matrix/fiber interface systems in LAMMPS format (Figure 3a) (~60,000 atoms in each simulation). While combining both structures, a 5 Å gap was purposely included to avoid overlap of atoms. Interaction between the matrix and fiber was evaluated using van der Waals interactions. Prior to thermal conductance simulations, all combined systems were equilibrated for 200, 2000, and 200 ps in *NVT*, *NPT*, and *NVE* ensembles, respectively, with respective time steps of 1, 1, and 0.5 fs. We should point out that, during equilibration, the orientation angle for *C*₉₀ cases was eventually equilibrated to ~83°, while orientation angles for other graphitic cases did not change to a noticeable degree.

2.5. Interface Thermal Conductance Calculations. The thermal conductance across BMI-matrix surface-carbon models' interfaces was calculated using nonequilibrium molecular dynamics (NEMD) simulations from a slab-like geometry based on Fourier law approach⁴⁸ and is also schematically depicted in Figure 3b. As seen from the figure, the outer edges of the elongated slab (1 nm) were fixed, while the adjacent 1.5 nm bins were employed as hot and cold thermostats, where a temperature rescaling algorithm was employed to keep the respective temperatures to 350 and 250 K. *NVE* ensemble was employed for nonthermostated regions. In order to keep the regions at their specified temperatures, energy was continuously added and taken off from the hot and cold regions, respectively. Our previous

studies on silicon and polymer composites have shown that thermal conductivity and interface thermal conductance prediction is not noticeably affected by choice of thermostats (Nose–Hoover, Berendsen, and temperature rescaling).^{49–51}

By applying thermostats, a temperature gradient is established over time along the elongated slab direction, leading to a steady-state temperature profile. Furthermore, near the interface, a temperature discontinuity develops due to a mismatch between the vibrational properties of the two media. The temperature profile can then be calculated by dividing the slab into a predefined number of thin slabs with equal thickness (2 Å for our case) and calculating the temperature of each bin using the following equation.

$$T_i = \frac{1}{3N_i k_B} \sum_{k=1}^{N_i} m_k v_k^2 \quad (1)$$

where *N_i* is the number of atoms in the *i*th slab and *m_k* and *v_k* correspond to atomic mass and velocity of atom *k*, respectively. For the current study, each of the 2 Å bins contained ~500 atoms. As an example, one such steady-state temperature profile for a representative case is shown in Supporting Information section S5 along with the calculation of temperature discontinuity, Δ*T*. The interface thermal conductance was then calculated using the following equation.

$$\Lambda = \frac{Q}{A\Delta T} \quad (2)$$

where Λ, *A*, and *Q* respectively correspond to interface thermal conductance, cross-sectional area, and heat flux as estimated by the energy dumped into hot (taken out from cold) thermostats.⁵² The heat flux calculation is further discussed in Supporting Information section S6 using the cumulative energy dumped (or taken out) estimates for a representative case. For all cases, initial simulations were run for about 1 ns in order to achieve steady-state. Following that, simulations were further run for 4 ns for data collection for temperature gradient and heat flux calculations.

3. RESULTS AND DISCUSSION

Next, we present and discuss the effect of various parameters on thermal transport across the carbon-fiber/matrix interface. Here, unlike the previous section, we have not divided the discussion between carbon-surface and interface models but have attempted to present the effect of different build models in a more coherent way. We wrap up this section with a few comments on possible modifications to interface thermal conductance due to matrix cross-linking, which is not investigated in this study.

3.1. Effect of Functionalization. We start this section with discussing the effect of surface functionalization density on interface thermal conductance as shown in Figure 4. The figure clearly shows that the interface functionalization significantly increases the thermal conductance across the interface with respect to unfunctionalized interface (*C*₉₀), increasing up to 4-fold for surface functionalization density of 0.55 molecules/nm². The increasing trend and relative increase is in excellent agreement with the previous literature.^{18,20,23,24,27,29,30} Here, the increase in thermal conductance is attributed to the interface bonding which provides additional pathways via covalent bonds, in addition to van der Waals interactions, for better thermal energy transport across the interface.

The surface functionalization is expected to occur via “end atoms” of polymeric fragments, whose volumetric concentration for oligomeric or polymeric chains is expected to be <<1 nm³. In this context, we believe that the largest modeled surface functionalization density of 0.55 molecules/nm² is noticeably higher than experimentally achievable surface functionalization densities of attaching amorphous polymeric fragments on

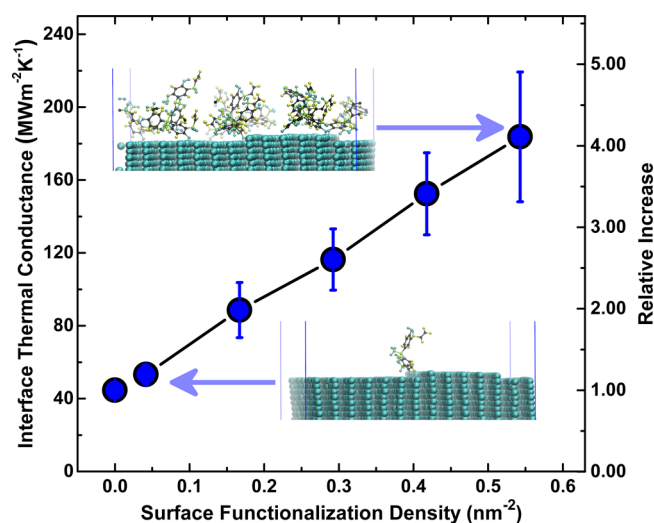


Figure 4. Plot of interface thermal conductance as a function of surface functionalization density for studied functionalized cases. Two schematics of functionalized interface are also shown. Relative increase in conductance with respect to unfunctionalized C_{90} case is plotted as well.

carbon-fiber surfaces. Thus, current study provides an estimate of conductance enhancement bounds, achievable in realistic experimental conditions.

3.2. Effect of Interface Roughness. Generally, when dealing with rough interfaces, there is an overlap region where both components (carbon-fiber surface and matrix in our case) are present. Estimating thermal transport across such cases introduces the concept of “interphase” as the definition of “interface” or a distinct “plane” becomes blurry. Such behavior is depicted in Figure 5 for one of our model systems which shows the presence of both graphitic carbon and matrix overlap over a 3 nm region. In principle, one could define various “planes” or “interfaces” (as depicted in Figure 5), but such a

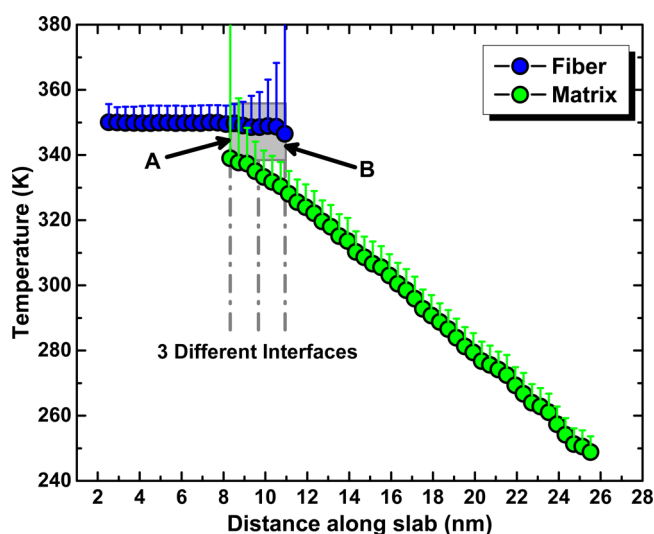


Figure 5. Plot of steady-state temperature profile across rough interfaces along the slab direction. Three different interfaces are depicted within the rough interphase with dashed–dotted lines and are discussed in Supporting Information section S7. “A” and “B” denote opposite boundaries of the interphase. Only the upper halves of the error bars are shown for clarity purposes.

definition is arbitrary and leads to different values of interface thermal conductance based on the chosen interface (please see Supporting Information section S7 for further discussion). In order to avoid that ambiguity, we calculate interphase thermal conductance between points A and B, which denote the boundaries of the interphase region, as shown in Figure 5. The resulting interphase thermal conductance is plotted in Figure 6

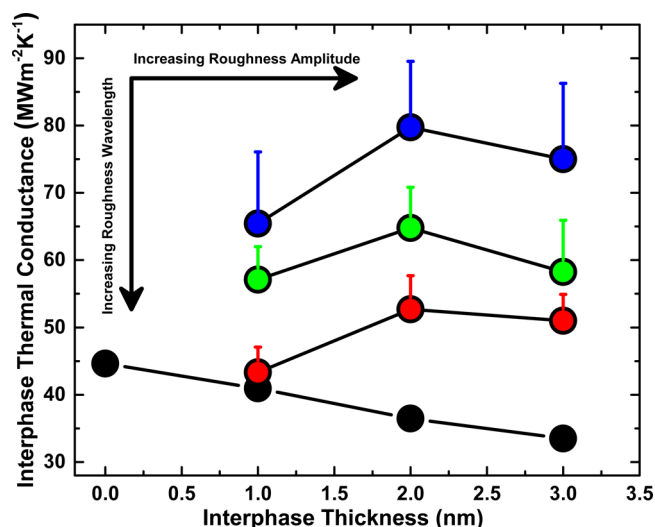


Figure 6. Plot of interphase thermal conductance as a function of interphase thickness for three different roughness wavelengths of 5 (red), 2.5 (green), and 1.7 nm (blue). Black data points show “effective” thermal conductance across the same width for the flat C_{90} graphitic model. Only the upper halves of the error bars are shown for clarity purposes.

as a function of interphase width for three different wavelength periodicities and compares the modulation with respect to the thermal conductance of a flat interface (C_{90}) for similar width (black data points).

For a constant interface width, the data show that the thermal conductance increases with decreasing periodicity. This increase can be attributed to an increase in carbon-fiber surface area which interacts with the matrix, leading to enhanced thermal conduction. For modeled interface widths, our simulations show a relative increase by a factor of 2–3 in thermal conductance with respect to their flat counterpart. For a constant wavelength, however, the data show that the interphase thermal conductance does not alter significantly and does not show a clear trend with increase in interphase width (or roughness amplitude). While increase in interphase width increases total thermal energy exchange (increase in surface area), it also increases the width over which the thermal conductance is estimated. These two features compete against each other in interphase thermal conductance estimation (increase in both numerator and denominator), leading to an overall minor variation in Figure 6. Nevertheless, it is important to note the relative increase in thermal conductance with respect to flat interfaces as a function of roughness amplitude as well as periodicity of roughness undulation.

3.3. Effect of CNT Incorporation at the Interface.

Similar to roughness, incorporation of CNTs at the carbon-fiber/matrix interface reignites the conductance discussion in terms of interphase. In this context, Figure 7 (inset) shows the estimated thermal conductance across the interphase as depicted by points A (fused junction) and B (nanotube cap).

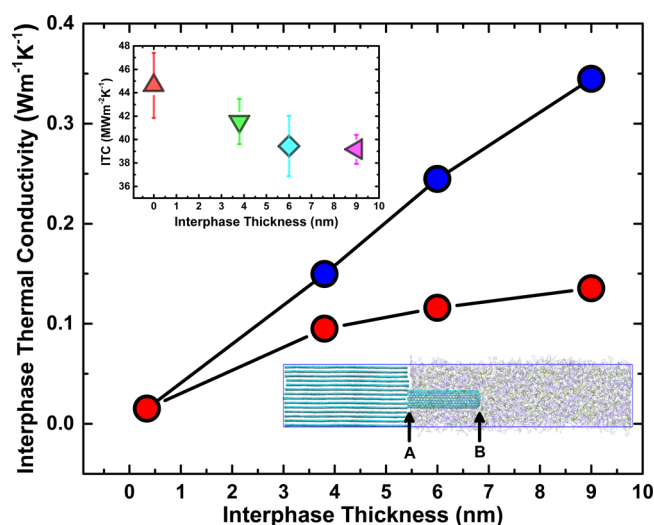


Figure 7. Plot of interphase thermal conductivity as a function of interphase thickness (or CNT length). Blue data points show thermal conductivity of CNT-bonded interphases for different widths while red data points show “effective” thermal conductivity for the same widths for the flat C_{90} graphitic model with no CNTs. Inset: Plot of interphase thermal conductance as a function of interphase thickness for four different studied cases: flat interface (red); 3.8 nm CNT (green); 6 nm CNT (cyan); 9 nm CNT (pink).

Over a length of 9 nm, only a slight decrease in conductance is observed which is indicative of a more conductive interphase and is attributed to an increase in effective surface area for thermal energy transport.⁵³ The ramifications of this slight decrease are further substantiated in Figure 7 (main) which plots the interphase thermal conductivity as a function of interphase thickness. Also shown in the same plot is the estimated thermal conductivity of the same region (including the interface) if only the matrix were present. In addition to the increase in effective thermal conductivity of the interface with CNT length, the figure shows that this increase is also noticeable (up to 2-fold for modeled cases) with respect to the effective thermal conductivity of the pure matrix in that region. Based on the observed trends, it is expected that higher surface density and a longer length of covalently bonded CNTs at carbon-fiber surfaces can greatly enhance thermal transport properties across the fiber/matrix interface.

3.4. Effect of Fiber Surface Morphology Thickness. For high thermal conductivity materials, such as CNTs and graphite, it has repeatedly been shown that the system size of MD simulations affects the prediction of thermal transport properties because of their extremely large phonon mean free paths.^{46,49,54,55} For our system, modeled graphitic surfaces of 10 nm also present a similar scenario. In order to investigate if the thickness of graphitic surface models (equivalent to mimicking the thickness of carbon-fiber surface morphology) has a consequential effect on interfacial thermal transport, we modeled several graphitic lengths for the C_{33} model system. In this context, Figure 8 shows the calculated thermal conductance values for different studied lengths ranging from ~ 5 to ~ 17 nm. The figure clearly shows that interface thermal conductance does increase significantly with increasing graphitic length. The primary reason behind such an increase is attributed to the inclusion of longer wavelength phonons within the graphitic model with increasing thickness, which can couple with the BMI matrix when they propagate to the interface.

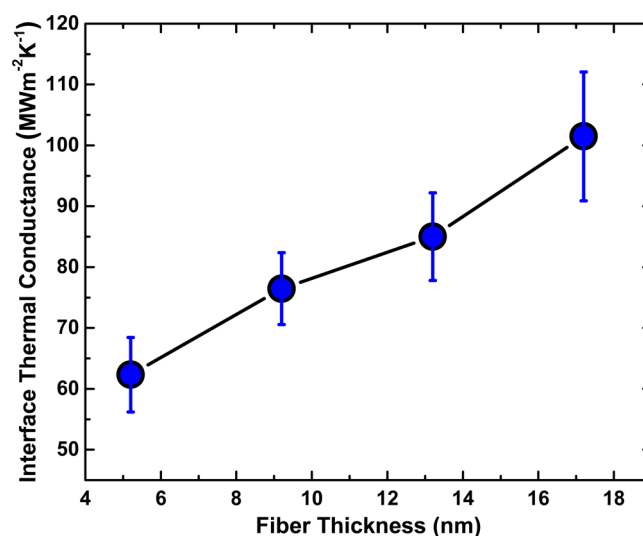


Figure 8. Plot of interface thermal conductance as a function of effective fiber thickness for the C_{33} graphitic model case.

While the simulations were performed for 10 s of nm of graphitic thickness, the conductance values are expected to saturate eventually, when fiber dimensions exceed characteristics mean free path of in-plane phonons in graphite ($\sim \mu\text{m}$).

3.5. Effect of Graphitic Orientation. Next, we discuss how the orientation of graphitic layers can modulate the thermal energy transport across the interphase. In this context, Figure 9 plots and shows the monotonic decrease of the

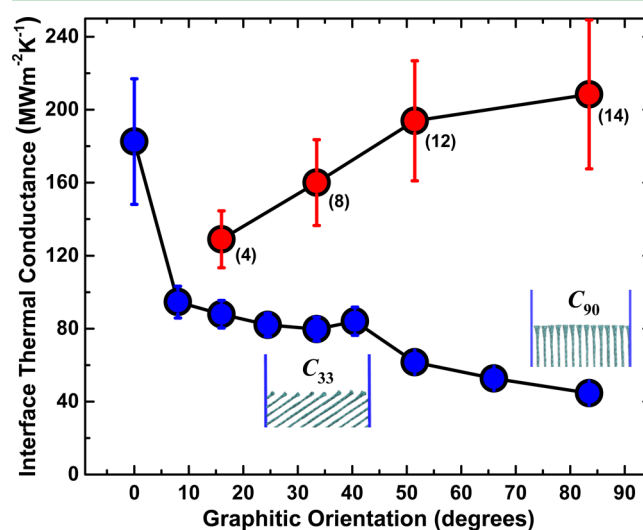


Figure 9. Plot of interface thermal conductance as a function of graphitic orientation for unsaturated (blue) and saturated (red) interface bonds. The numbers next to the red data points show the number of graphene layer edges at the interface. As the graphitic orientation angle increases, so do the number of graphene layer edges. Two schematics for C_{33} and C_{90} graphitic models demonstrate the said increase in graphene layer edges.

estimated interface thermal conductance as a function of graphitic orientation angle, θ . For clearer interpretation, we separate our discussion into 0° (C_0) and non- 0° (C_8 – C_{90}) graphitic orientation cases. The reason being that for C_8 – C_{90} cases, graphene layers interacting with the matrix are directly connected to the hot thermostat, while for the C_0 case, energy

has to propagate from the hot thermostated graphene layers to the end-graphene surface directly interacting with the matrix through in-between mediating graphene layers via van der Waals interactions (See [Supporting Information](#) section S8 for better pictorial visualization).

First, the exceptionally large value ($183 \text{ MWm}^{-2} \text{ K}^{-1}$) of interface thermal conductance for case C_0 is attributed to soft low-frequency modes propagating across graphene layers. These low-frequency modes can couple to a greater extent with the low-frequency vibrational modes of the matrix leading to enhanced thermal transport. Recent experiments on radial thermal transport across large multiwall CNTs have suggested the phonon mean free path across the out-of-plane direction of graphite to be $>100 \text{ nm}$.⁵⁶ In view of that, it is expected that the predicted conductance, based on 10 nm graphitic thickness, is expected to increase notably for much thicker flat graphitic ($\sim 0^\circ$) carbon-fiber surfaces.

On the other extreme, thermal conductance for perpendicular orientation (C_{90}) was observed to be ~ 5 -fold lower ($\sim 40 \text{ MWm}^{-2} \text{ K}^{-1}$) for the same model thickness of $\sim 10 \text{ nm}$. The low value is attributed to the small thickness (10 nm) as well as relatively stiff (high-frequency) propagating modes. When such phonons reach the interface, the probability of their reflection at the interface is greater than soft out-of-plane modes of graphite (in the 0° case), leading to a lower value of thermal conductance. [Figure 9](#) also shows that interface thermal conductance is increasing with decreasing θ for C_8 – C_{90} cases. This increase in conductance is attributed to an increase in the “effective length” of the graphite ($L/\sin(\theta)$). Please see [Supporting Information](#) section S8 for visualization of the “effective length”. In these cases, phonons predominantly propagate along graphitic planes (in-plane modes) due to the extremely high thermal anisotropy of graphite (>100 times) before reaching graphene edges, which eventually dictate the thermal transport.

3.6. Effect of Interface Bond Saturation. [Figure 9](#) also shows the interface thermal conductance for four different graphitic orientations (C_{16} , C_{33} , C_{55} , and C_{90}) where we saturated the edge carbon atoms by hydrogen atoms (H atoms). First, for constant graphitic orientation, the [figure](#) shows that saturated models always show higher thermal conductance than their unsaturated counterpart. The added H atoms contribute toward enhancing van der Waals interactions, while taking minimal volume (small σ and short C–H bond length), resulting in a relative increase of conductance.

On the contrary, unlike unsaturated cases, we see an increase in conductance with increase in graphitic orientation angle. We attribute this increasing trend to the increasing number density of interacting atoms (H atoms) with the matrix near the interface. As noted in the [figure](#), the number of interacting graphene layers’ edges increase with an increase in orientation angle, which in turn also increases the surface number density of H atoms, leading to enhanced van der Waals interactions (the interactions scale as N^2 , N being the number of interacting atoms). Despite the shorter effective length for large θ models, enhanced interactions dominate and lead to an increase in conductance, also increasing the respective gap between saturated and unsaturated cases. We should note that while this is a somewhat hypothetical set of simulations, it does provide important information on how the number density of surface interacting atoms can modulate interface thermal conductance.

3.7. Effect of Graphitic Defects. Similar to graphitic orientation, the defects within carbon-fiber surface models can also affect interface thermal conductance as shown in [Figure 10](#).

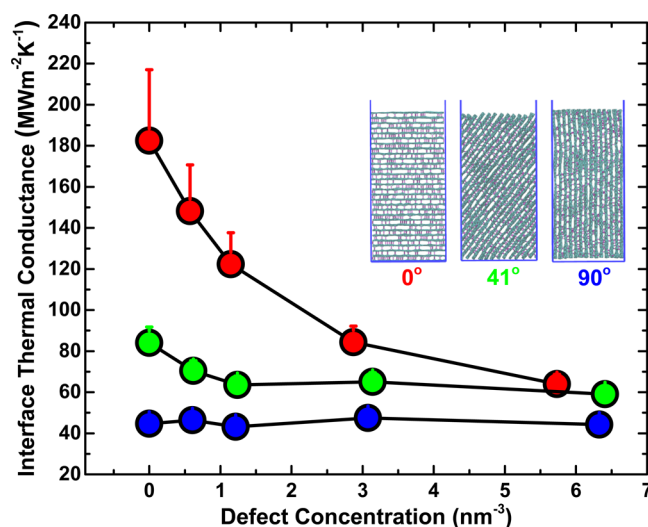


Figure 10. Plot of interface thermal conductance as a function of sp^3 defect concentrations for three different studied graphitic models, C_0 , C_{41} , and C_{90} . Schematics of these models for $\sim 3\%$ defect concentrations are shown for further visual clarity. Furthermore, only the upper halves of the error bars are shown for clarity purposes.

The [figure](#) shows significant decrease ($\sim 60\%$) in conductance for the C_0 model with respect to modeled defect concentrations, while the decrease is relatively minor for C_{41} ($\sim 20\%$) and C_{90} ($\sim 0\%$) graphitic models. For the former, the notable decrease is attributed to increased perturbation in coherency of out-of-plane modes with increased defect concentrations as these defects (sp^3) significantly reduce the phonon mean free path along the out-of-plane direction. However, for latter models (C_{41} and C_{90}), the minor or negligible decrease is associated with the observation that, in these cases, sp^3 bonds are orientated perpendicular to the dominant thermal transport direction (along graphene direction), minimally perturbing the energy carrying propagating phonons.

3.8. Effect of Matrix Cross-Linking on Interface Thermal Conductance. Similar to intrinsic fiber properties and interface features, it is expected that matrix properties (cured vs uncured) would also affect interface thermal conductance. However, this parameter space, i.e., effect of curing, is not explored in this study. Unlike modeling of an epoxy-based matrix curing process, which often requires modeling a single amine–epoxy reaction,⁵⁷ modeling the curing process of BMI-5292 resin involves five separate reactions (ene reaction, maleimide homopolymerization, alternating maleimide–adduct co-polymerization, ene adduct homopolymerization via propenyl groups, and dehydration/etherification reaction) leading to a much more complex curing pathway.^{31,32} The framework for the curing process involving all five reactions is currently being formulated using atomistic molecular dynamics simulations and would be reported in future studies. Nevertheless, based on our previous studies on interface thermal conductance across cured epoxy matrix and carbon nanotubes, we foresee that the curing process is expected to enhance the thermal conductance up to 20% .²⁴

4. CONCLUSIONS

In a single comprehensive investigation, this study explores a series of carbon-fiber bulk and interface parameters in order to gauge their importance toward engineering thermal transport across carbon-fiber/matrix interfaces. Based on atomistic molecular dynamics simulations, it is suggested that the long-range graphitic nature of carbon-fibers near the interface, a higher number density of surface atoms, a larger degree of functionalization, molecular surface roughness, and incorporation of high-conductivity fillers (such as CNTs) can significantly augment the interface thermal conductance across the interface. On the contrary, defects within the carbon fiber, low number density of interacting atoms, and less effective area of interaction due to voids (not studied here) can lead to a noticeable decrease in thermal conductance. In summary, the presented results provide key insights into realistic bounds (degree of variation) to the interface thermal conductance values at fiber/matrix interfaces as a function of many different surface-carbon morphologies. In addition, we believe that this parametric study incorporating various key parameters has broader ramifications on modulating thermal conductance, not only across carbon-fiber/matrix interfaces but also in different types of thermal interface materials as well as different nanoscopic devices where thermal dissipation plays a crucial role in device performance.

■ ASSOCIATED CONTENT

Supporting Information

The Supporting Information is available free of charge on the ACS Publications website at DOI: 10.1021/acsami.5b08591.

Detailed specifics on the generation of different carbon-surface models, estimation of the heat flux and the temperature drop across the interface, consequences of using an arbitrary interface for interface thermal conductance calculations for rough interfaces, and visual representation of differences between C_0 and C_8 – C_{90} graphitic orientation cases with respect to applied thermostats (PDF)

■ AUTHOR INFORMATION

Corresponding Authors

*(V.V.) E-mail: vikas.varshney@wpafb.af.mil.

*(J.W.B.) E-mail: jeffery.baur@us.af.mil.

Notes

The authors declare no competing financial interest.

■ ACKNOWLEDGMENTS

We acknowledge the U.S. Air Force Office of Scientific Research (AFOSR) for financial support (Grant No. 13RXCOR; Program Manager, Dr. B. L. "Les" Lee) and the Department of Defense Supercomputing Research Center (AFRL-DSRC and ERDC-DSRC) for computational resources to carry out the simulations.

■ REFERENCES

- (1) El-Aneel, A.; Cohen, A.; Banoub, J. Mass Spectrometry, Review of the Basics: Electrospray, MALDI, and Commonly Used Mass Analyzers. *Appl. Spectrosc. Rev.* **2009**, *44*, 210–230.
- (2) Zhang, Y.-L.; Chen, Q.-D.; Xia, H.; Sun, H.-B. Designable 3D Nanofabrication by Femtosecond Laser Direct Writing. *Nano Today* **2010**, *5*, 435–448.

- (3) Kabashin, A.; Delaporte, P.; Pereira, A.; Grojo, D.; Torres, R.; Sarnet, T.; Sentis, M. Nanofabrication with Pulsed Lasers. *Nanoscale Res. Lett.* **2010**, *5*, 454–463.
- (4) Conforti, P. F.; Prasad, M.; Garrison, B. J. Elucidating the Thermal, Chemical, and Mechanical Mechanisms of Ultraviolet Ablation in Poly(methyl methacrylate) via Molecular Dynamics Simulations. *Acc. Chem. Res.* **2008**, *41*, 915–924.
- (5) Lippert, T.; Dickinson, J. T. Chemical and Spectroscopic Aspects of Polymer Ablation: Special Features and Novel Directions. *Chem. Rev.* **2003**, *103*, 453–86.
- (6) Han, Z.; Fina, A. Thermal Conductivity of Carbon Nanotubes and Their Polymer Nanocomposites: A Review. *Prog. Polym. Sci.* **2011**, *36*, 914–944.
- (7) McNamara, A. J.; Joshi, Y.; Zhang, Z. M. Characterization of Nanostructured Thermal Interface Materials – A Review. *Int. J. Therm. Sci.* **2012**, *62*, 2–11.
- (8) Hung, M. T.; Choi, O.; Ju, Y. S.; Hahn, H. T. Heat Conduction in Graphite-Nanoplatelet-Reinforced Polymer Nanocomposites. *Appl. Phys. Lett.* **2006**, *89*, 023117.
- (9) Huang, J.; Gao, M.; Pan, T.; Zhang, Y.; Lin, Y. Effective Thermal Conductivity of Epoxy Matrix Filled with Poly(ethyleneimine) Functionalized Carbon Nanotubes. *Compos. Sci. Technol.* **2014**, *95*, 16–20.
- (10) Zhang, P.; Li, Q.; Xuan, Y. Thermal Contact Resistance of Epoxy Composites Incorporated with Nano-Copper Particles and the Multi-Walled Carbon Nanotubes. *Composites, Part A* **2014**, *57*, 1–7.
- (11) Gharagozloo-Hubmann, K.; Boden, A.; Czempel, G. J. F.; Firkowska, I.; Reich, S. Filler Geometry and Interface Resistance of Carbon Nanofibers: Key Parameters in Thermally Conductive Polymer Composites. *Appl. Phys. Lett.* **2013**, *102*, 213103.
- (12) Lizundia, E.; Oleaga, A.; Salazar, A.; Sarasua, J. R. Nano- and Microstructural Effects on Thermal Properties of Poly (L-lactide)/ Multi-Wall Carbon Nanotube Composites. *Polymer* **2012**, *53*, 2412–2421.
- (13) Yu, J.; Tonpheng, B.; Gröbner, G.; Andersson, O. Thermal Properties and Transition Studies of Multi-Wall Carbon Nanotube/ Nylon-6 Composites. *Carbon* **2011**, *49*, 4858–4866.
- (14) Roy, A. K.; Farmer, B. L.; Varshney, V.; Sih, S.; Lee, J.; Ganguli, S. Importance of Interfaces in Governing Thermal Transport in Composite Materials: Modeling and Experimental Perspectives. *ACS Appl. Mater. Interfaces* **2012**, *4*, 545–563.
- (15) Frenkel, D.; Smit, B. *Understanding Molecular Simulation: From Algorithms to Applications*. Academic Press: London, 2001; Vol. 1.
- (16) Huxtable, S. T.; Cahill, D. G.; Shenogin, S.; Xue, L.; Ozisik, R.; Barone, P.; Usrey, M.; Strano, M. S.; Siddons, G.; Shim, M.; Keblinski, P. Interfacial Heat Flow in Carbon Nanotube Suspensions. *Nat. Mater.* **2003**, *2*, 731–734.
- (17) Shenogin, S.; Xue, L.; Ozisik, R.; Keblinski, P.; Cahill, D. G. Role of Thermal Boundary Resistance on the Heat Flow in Carbon-Nanotube Composites. *J. Appl. Phys.* **2004**, *95*, 8136–8144.
- (18) Shenogin, S.; Bodapati, A.; Xue, L.; Ozisik, R.; Keblinski, P. Effect of Chemical Functionalization on Thermal Transport of Carbon Nanotube Composites. *Appl. Phys. Lett.* **2004**, *85*, 2229–2232.
- (19) Unnikrishnan, V.; Reddy, J.; Banerjee, D.; Rostam-Abadi, F. Thermal Characteristics of Defective Carbon Nanotube-Polymer Nanocomposites. *Interact. Multiscale Mech.* **2008**, *1*, 397–409.
- (20) Konatham, D.; Striolo, A. Thermal Boundary Resistance at the Graphene-Oil Interface. *Appl. Phys. Lett.* **2009**, *95*, 163105.
- (21) Luo, T.; Lloyd, J. R. Enhancement of Thermal Energy Transport across Graphene/Graphite and Polymer Interfaces: A Molecular Dynamics Study. *Adv. Funct. Mater.* **2012**, *22*, 2495–2502.
- (22) Hida, S.; Hori, T.; Shiga, T.; Elliott, J.; Shiomi, J. Thermal Resistance and Phonon Scattering at the Interface between Carbon Nanotube and Amorphous Polyethylene. *Int. J. Heat Mass Transfer* **2013**, *67*, 1024–1029.
- (23) Lin, S.; Buehler, M. J. The Effect of Non-Covalent Functionalization on the Thermal Conductance of Graphene/Organic Interfaces. *Nanotechnology* **2013**, *24*, 165702.

- (24) Varshney, V.; Roy, A. K.; Michalak, T. J.; Lee, J.; Farmer, B. L. Effect of Curing and Functionalization on the Interface Thermal Conductance in Carbon Nanotube–Epoxy Composites. *JOM* **2013**, *65*, 140–146.
- (25) Merabia, S.; Termentzidis, K. Thermal Boundary Conductance across Rough Interfaces Probed by Molecular Dynamics. *Phys. Rev. B: Condens. Matter Mater. Phys.* **2014**, *89*, 054309.
- (26) Kuang, Y.; Huang, B. Effects of Covalent Functionalization on the Thermal Transport in Carbon Nanotube/Polymer Composites: A Multi-Scale Investigation. *Polymer* **2015**, *56*, S63–S71.
- (27) Wang, M.; Hu, N.; Zhou, L.; Yan, C. Enhanced Interfacial Thermal Transport across Graphene–Polymer Interfaces by Grafting Polymer Chains. *Carbon* **2015**, *85*, 414–421.
- (28) Liu, Y.; Hu, C.; Huang, J.; Sumpter, B. G.; Qiao, R. Tuning Interfacial Thermal Conductance of Graphene Embedded in Soft Materials by Vacancy Defects. *J. Chem. Phys.* **2015**, *142*, 244703.
- (29) Ni, Y.; Han, H.; Volz, S.; Dumitrică, T. Nanoscale Azide Polymer Functionalization: A Robust Solution for Suppressing the Carbon Nanotube–Polymer Matrix Thermal Interface Resistance. *J. Phys. Chem. C* **2015**, *119*, 12193–12198.
- (30) Wang, Y.; Zhan, H. F.; Xiang, Y.; Yang, C.; Wang, C. M.; Zhang, Y. Y. Effect of Covalent Functionalization on Thermal Transport across Graphene–Polymer Interfaces. *J. Phys. Chem. C* **2015**, *119*, 12731–12738.
- (31) Rozenberg, B. A.; Boiko, G. N.; Morgan, R. J.; Shin, E. E. The Cure Mechanism of the 4,4'-(N,N'-Bismaleimide)diphenylmethane-2,2'-diallylbisphenol A System. *Polym. Sci., Ser. A* **2001**, *43*, 630–645.
- (32) Rozenberg, B. A.; Dzhavadyan, E. A.; Morgan, R.; Shin, E. High-Performance Bismaleimide Matrices: Cure Kinetics and Mechanism. *Polym. Adv. Technol.* **2002**, *13*, 837–844.
- (33) Cho, D.; Drzal, L. T. Effect of Thermal Cure on the Fluorescence of Matrimid 5292 Bismaleimide Resin. *J. Mater. Sci. Lett.* **2003**, *22*, 459–461.
- (34) Lincoln, J. E.; Morgan, R. J.; Shin, E. E. Moisture Absorption-Network Structure Correlations in BMPM/DABPA Bismaleimide Composite Matrices. *J. Adv. Mater.* **2000**, *32*, 24–34.
- (35) *Materials Studio*; Accelrys Software: San Diego, CA, USA, 2012.
- (36) Dauber-Osguthorpe, P.; Roberts, V. A.; Osguthorpe, D. J.; Wolff, J.; Genest, M.; Hagler, A. T. Structure and Energetics of Ligand Binding to Proteins: Escherichia Coli Dihydrofolate Reductase-Trimethoprim, a Drug-Receptor System. *Proteins: Struct., Funct., Genet.* **1988**, *4*, 31–47.
- (37) Sun, H.; Mumby, S. J.; Maple, J. R.; Hagler, A. T. An Ab Initio CFF93 All-Atom Force Field for Polycarbonates. *J. Am. Chem. Soc.* **1994**, *116*, 2978–2987.
- (38) Wang, J.; Wolf, R. M.; Caldwell, J. W.; Kollman, P. A.; Case, D. A. Development and Testing of a General Amber Force Field. *J. Comput. Chem.* **2004**, *25*, 1157–1174.
- (39) Cornell, W. D.; Cieplak, P.; Bayly, C. I.; Gould, I. R.; Merz, K. M.; Ferguson, D. M.; Spellmeyer, D. C.; Fox, T.; Caldwell, J. W.; Kollman, P. A. A Second Generation Force Field for the Simulation of Proteins, Nucleic Acids, and Organic Molecules. *J. Am. Chem. Soc.* **1995**, *117*, 5179–5197.
- (40) Frisch, M. J.; Trucks, G. W.; Schlegel, H. B.; Scuseria, G. E.; Robb, M. A.; Cheeseman, J. R.; Scalmani, G.; Barone, V.; Mennucci, B.; Petersson, G. A.; Nakatsuji, H.; Caricato, M.; Li, X.; Hratchian, H. P.; Izmaylov, A. F.; Bloino, J.; Zheng, G.; Sonnenberg, J. L.; Hada, M.; Ehara, M.; Toyota, K.; Fukuda, R.; Hasegawa, J.; Ishida, M.; Nakajima, T.; Honda, Y.; Kitao, O.; Nakai, H.; Vreven, T.; Montgomery, J. A., Jr.; Peralta, J. E.; Ogliaro, F. O.; Bearpark, M. J.; Heyd, J.; Brothers, E. N.; Kudin, K. N.; Staroverov, V. N.; Kobayashi, R.; Normand, J.; Raghavachari, K.; Rendell, A. P.; Burant, J. C.; Iyengar, S. S.; Tomasi, J.; Cossi, M.; Rega, N.; Millam, N. J.; Klene, M.; Knox, J. E.; Cross, J. B.; Bakken, V.; Adamo, C.; Jaramillo, J.; Gomperts, R.; Stratmann, R. E.; Yazyev, O.; Austin, A. J.; Cammi, R.; Pomelli, C.; Ochterski, J. W.; Martin, R. L.; Morokuma, K.; Zakrzewski, V. G.; Voth, G. A.; Salvador, P.; Dannenberg, J. J.; Dapprich, S.; Daniels, A. D.; Farkas, A. d. n.; Foresman, J. B.; Ortiz, J. V.; Cioslowski, J.; Fox, D. J. *Gaussian 09*, Revision A.02; Gaussian: Wallingford, CT, USA, 2009.
- (41) Dupradeau, F.-Y.; Pigache, A.; Zaffran, T.; Savineau, C.; Lelong, R.; Grivel, N.; Lelong, D.; Rosanski, W.; Cieplak, P. The R.E.D. Tools: Advances in RESP and ESP Charge Derivation and Force Field Library Building. *Phys. Chem. Chem. Phys.* **2010**, *12*, 7821–7839.
- (42) Plimpton, S. Fast Parallel Algorithms for Short-Range Molecular Dynamics. *J. Comput. Phys.* **1995**, *117*, 1–19.
- (43) Varshney, V.; Roy, A. K.; Baur, J. Molecular Modeling of BMI Matrix, Its Thermo-Physical Properties, and Its Interface with Amorphous Carbon Fiber. In *Proceedings of the American Society for Composites 2014—Twenty-ninth Technical Conference on Composite Materials*, San Diego, CA, USA, Sep. 17, 2014; Kim, K.; Whisler, D.; Chen, Z. M.; Bisagni, C.; Kawai, M.; Krueger, R., Eds.; DEStech Publications: San Diego, CA, USA, 2014.
- (44) Loh, G. C.; Baillargeat, D. Graphitization of Amorphous Carbon and Its Transformation Pathways. *J. Appl. Phys.* **2013**, *114*, 033534.
- (45) We tried different approaches using AIREBO and Tersoff potentials to create graphitic order from amorphous carbon as discussed by ref 44 but were not successful in repeatedly reproducing the graphitic order. Hence we chose to add defects in pristine graphite.
- (46) Pop, E.; Varshney, V.; Roy, A. K. Thermal Properties of Graphene: Fundamentals and Applications. *MRS Bull.* **2012**, *37*, 1273–1281.
- (47) Robinson, M.; Marks, N. A. NanoCap: A Framework for Generating Capped Carbon Nanotubes and Fullerenes. *Comput. Phys. Commun.* **2014**, *185*, 2519–2526.
- (48) Anderson, C. V. D. R.; Tamma, K. K. An Overview of Advances in Heat Conduction Models and Approaches for Prediction of Thermal Conductivity in Thin Dielectric Films. *Int. J. Numer. Methods Heat Fluid Flow* **2004**, *14*, 12–65.
- (49) Varshney, V.; Roy, A. K.; Froudakis, G.; Farmer, B. L. Molecular Dynamics Simulations of Thermal Transport in Porous Nanotube Network Structures. *Nanoscale* **2011**, *3*, 3679–3684.
- (50) Varshney, V.; Roy, A. K.; Dudis, D. S.; Lee, J.; Farmer, B. L. A Novel Nano-Configuration for Thermoelectrics: Helicity Induced Thermal Conductivity Reduction in Nanowires. *Nanoscale* **2012**, *4*, 5009–5016.
- (51) Varshney, V.; Lee, J.; Farmer, B. L.; Voevodin, A. A.; Roy, A. K. Modeling of Cross-Plane Interface Thermal Conductance between Graphene Nano-Ribbons. *2D Mater.* **2014**, *1*, 025005.
- (52) After steady-state is reached, net heat flux is calculated by taking the slope of the cumulative energy output dumped by LAMMPS as discussed in [Supporting Information](#) section S6.
- (53) For a constant thermal conductivity interphase, thermal conductance decreases inversely with thickness. The observation that the decrease in thermal conductance is minimal over an ~10-fold increase in interphase thickness is indicative of an increasing thermally conductive interphase.
- (54) Marconnet, A. M.; Panzer, M. A.; Goodson, K. E. Thermal Conduction Phenomena in Carbon Nanotubes and Related Nanostructured Materials. *Rev. Mod. Phys.* **2013**, *85*, 1295–1326.
- (55) Varshney, V.; Patnaik, S. S.; Roy, A. K.; Froudakis, G.; Farmer, B. L. Modeling of Thermal Transport in Pillared-Graphene Architectures. *ACS Nano* **2010**, *4*, 1153–1161.
- (56) Yang, J.; Shen, M.; Yang, Y.; Evans, W. J.; Wei, Z.; Chen, W.; Zinn, A. A.; Chen, Y.; Prasher, R.; Xu, T. T.; Koblinski, P.; Li, D. Phonon Transport through Point Contacts between Graphitic Nanomaterials. *Phys. Rev. Lett.* **2014**, *112*, 205901.
- (57) Varshney, V.; Patnaik, S. S.; Roy, A. K.; Farmer, B. L. A Molecular Dynamics Study of Epoxy-Based Networks: Cross-Linking Procedure and Prediction of Molecular and Material Properties. *Macromolecules* **2008**, *41*, 6837–6842.